# Interspecies Interactions Stimulate Diversification of the Streptomyces coelicolor Secreted Metabolome

# Interspecies Interactions Stimulate Diversification of the *Streptomyces coelicolor* Secreted Metabolome

**Matthew F. Traxler,[a] Jeramie D. Watrous,[b,c,d] Theodore Alexandrov,[d,e] Pieter C. Dorrestein,[b,c,d,f] Roberto Kolter[a]**

Department of Microbiology and Immunobiology, Harvard Medical School, Boston, Massachusetts, USA[a]; Department of Pharmacology[b] and Department of Chemistry and Biochemistry,[c] University of California at San Diego, La Jolla, California, USA; Skaggs School of Pharmacy and Pharmaceutical Sciences, University of California at San Diego, La Jolla, California, USA[d]; Center for Industrial Mathematics, University of Bremen, Bremen, Germany[e]; Center for Marine Biotechnology and Biomedicine, Scripps Institution of Oceanography, University of California at San Diego, La Jolla, California, USA[f]

**ABSTRACT** **Soils host diverse microbial communities that include filamentous actinobacteria (actinomycetes). These bacteria have been a rich source of useful metabolites, including antimicrobials, antifungals, anticancer agents, siderophores, and immunosuppressants. While humans have long exploited these compounds for therapeutic purposes, the role these natural products may play in mediating interactions between actinomycetes has been difficult to ascertain. As an initial step toward understanding these chemical interactions at a systems level, we employed the emerging techniques of nanospray desorption electrospray ionization (NanoDESI) and matrix-assisted laser desorption ionization–time of flight (MALDI-TOF) imaging mass spectrometry to gain a global chemical view of the model bacterium *Streptomyces coelicolor* interacting with five other actinomycetes. In each interaction, the majority of secreted compounds associated with *S. coelicolor* colonies were unique, suggesting an idiosyncratic response from *S. coelicolor*. Spectral networking revealed a family of unknown compounds produced by *S. coelicolor* during several interactions. These compounds constitute an extended suite of at least 12 different desferrioxamines with acyl side chains of various lengths; their production was triggered by siderophores made by neighboring strains. Taken together, these results illustrate that chemical interactions between actinomycete bacteria exhibit high complexity and specificity and can drive differential secondary metabolite production.**

**IMPORTANCE** **Actinomycetes, filamentous actinobacteria from the soil, are the deepest natural source of useful medicinal compounds, including antibiotics, antifungals, and anticancer agents. There is great interest in developing new strategies that increase the diversity of metabolites secreted by actinomycetes in the laboratory. Here we used several metabolomic approaches to examine the chemicals made by these bacteria when grown in pairwise coculture. We found that these interspecies interactions stimulated production of numerous chemical compounds that were not made when they grew alone. Among these compounds were at least 12 different versions of a molecule called desferrioxamine, a siderophore used by the bacteria to gather iron. Many other compounds of unknown identity were also observed, and the pattern of compound production varied greatly among the interaction sets. These findings suggest that chemical interactions between actinomycetes are surprisingly complex and that coculture may be a promising strategy for finding new molecules from actinomycetes.**

**Received** 27 June 2013 **Accepted** 19 July 2013 **Published** 20 August 2013

**Citation** Traxler MF, Watrous JD, Alexandrov T, Dorrestein PC, Kolter R. 2013. Interspecies interactions stimulate diversification of the *Streptomyces coelicolor* secreted metabolome. mBio 4(4):e00459-13. doi:10.1128/mBio.00459-13.

**Editor** Julian Davies, University of British Columbia



Address correspondence to Roberto Kolter, rkolter@hms.harvard.edu, or Pieter C. Dorrestein, pdorrestein@ucsd.edu.

Actinomycetes remain the single richest source of medically useful natural products, including antibiotics, antifungals, anthelminthics, antitumor agents, and siderophores (1–4). Most actinomycetes dedicate a substantial fraction of their genomes to the production of such natural products (~4.5% in the case of *Streptomyces coelicolor*) (3, 5). Yet it is clear that the overwhelming majority of this biosynthetic potential is not expressed under standard laboratory conditions (3, 5, 6). Thus, there is great interest in developing new strategies that increase the number and diversity of the metabolites secreted by actinomycetes in the laboratory.

Despite the clinical usefulness of these natural products, the roles that they play for the producing bacterium remain largely unknown (7). Their secreted nature has long prompted the idea that they may mediate diverse interactions between bacteria, ranging from chemical warfare to potential roles in signaling (5, 8, 9). This idea raises the possibility that coculture of actinomycetes may offer an avenue for discovery of compounds not produced in monocultures. However, systematically evaluating this hypothesis using traditional chemical techniques has been technically challenging.

Cocultivating different species of soil bacteria results in dramatic physiological changes relative to results when the bacteria are grown as pure cultures. Ueda et al. found that cocultivation of actinomycetes frequently induced morphological development and antibiotic production (10). These changes were caused by the production of the siderophore desferrioxamine by the strain stimulating antibiotic production (11). We recently found that the converse of this phenomenon is also at play in actinomycete in-

teractions, i.e., that production of a siderophore that cannot be used by one strain can lead to impaired development due to a decrease in local iron availability (12, 13). Another recent work that mapped pairwise interactions among a set of 64 *Streptomyces* isolates concluded that outcomes of such interactions are mostly determined by metabolite production (14). Several other studies have examined interactions between streptomycetes and the common soil bacterium *Bacillus subtilis* (15–22). These studies have documented a number of different interaction modalities, including inhibition of streptomycete development (15, 18–20, 22), degradation of signaling compounds via secreted enzyme activity (15, 18), and alteration of streptomycete natural product biosynthesis (16, 17, 21, 22). Given that each actinomycete is probably capable of producing dozens of secreted metabolites and that interspecies interactions may influence production of these molecules, we sought an experimental framework that would allow us to systematically examine changes in the secreted metabolome during multiple pairwise interspecies interactions.

The nascent mass spectrometry (MS) techniques of nanospray desorption electrospray ionization (NanoDESI) and matrix-assisted laser desorption ionization–time of flight (MALDI-TOF) imaging have recently opened new ways of examining the exchange of secondary metabolites between interacting bacteria *in situ* (21–24). In the work described here, we used these tools to examine the changes in the secreted metabolome of the well-studied actinomycete *S. coelicolor* as it grew near other actinomycetes. We studied five such interactions, and in each case we found many metabolites that were not produced by *S. coelicolor* when grown as a pure culture. We also observed that the sets of metabolites associated with *S. coelicolor* colonies were highly variable depending on the interacting partner, suggesting a unique response in each case. Several interactions triggered the production of an extended family of acylated desferrioxamines, never before observed from *S. coelicolor*. Altogether, the results presented here indicate that interspecies interactions can trigger broad, differential production of secreted metabolites by a single streptomycete.

## RESULTS

**Experimental system for studying actinomycete interactions.** *S. coelicolor* is perhaps the best-studied actinomycete. Many features of its genome, secondary metabolism, growth, development, and stress response have been characterized (25–28). Some growth media, such as R2YE, stimulate rapid multicellular development of *S. coelicolor* and production of a range of secondary metabolites, including the pigmented antibiotics actinorhodin and the prodiginines (29). Other growth media, including ISP2 (International Streptomyces Project medium 2), support the growth of *S. coelicolor*, but robust development and secondary metabolite production occur only after prolonged incubation (i.e., >10 days). To look for interactions that stimulated such metabolite biosynthesis by *S. coelicolor* on ISP2 medium, we spotted 1 μl of an *S. coelicolor* spore suspension 5 mm from 20 similar inocula of other actinomycetes. Several actinomycetes triggered production of the red antibiotic prodiginine in *S. coelicolor*, in some cases as early as 3 days. For example, see the interaction with *Amycolatopsis* sp. AA4 in Fig. 1A. Of these 20 interactions, we focused on 5 (all shown in Fig. 1A) that provoked different temporal and phenotypic responses in *S. coelicolor* ranging from no stimulation of pigmentation or development (*Streptomyces* sp. E14 interaction) to partial or strong pigmentation (*Streptomyces* sp. SPB74 and *Amycolatopsis* sp. AA4 interactions, respectively) and both pigmentation and development (*Streptomyces albus* J1074 and *Streptomyces viridochromogenes* DSM40736 interactions). Given that developmental and natural product biosynthetic regulatory cascades are linked in *S. coelicolor*, we hypothesized that these different phenotypes expressed by *S. coelicolor* might be indicative of differences in the pattern of small molecules produced.

To test this hypothesis, we employed two metabolomic approaches, nanospray desorption electrospray ionization (NanoDESI) and microbial matrix-assisted laser desorption ionization–time of flight (MALDI-TOF) imaging mass spectrometry (IMS), to examine the chemical response of *S. coelicolor* in each of these interactions. Importantly, both techniques allow for sampling directly from colonies grown on an agar substrate (21, 23). NanoDESI MS is a recently developed methodology in which the solvent is delivered to the sample surface via a fused silica capillary (21). A second capillary draws the solvent (now containing dissolved analyte) off the sample surface and delivers it directly into the mass spectrometer such that a small liquid bridge (~1 μl) is constantly maintained on the sample surface between the two capillary ends. The analyte desorbed from the sample surface is then subjected to data-dependent tandem MS analysis, ultimately yielding individual tandem mass spectra for the hundreds to thousands of ions detectable within the sample. We thus used NanoDESI MS and MALDI-TOF IMS to analyze the colonies of the interactions shown in Fig. 1A. The general experimental and data analysis work flow is diagrammed in Fig. 1B. In every case, we sampled both the *S. coelicolor* colony and the interacting colony, which we refer to as the initiator colony, at days three, five, and seven. We also sampled control colonies of *S. coelicolor* that were grown in isolation on the same medium and at similar time points. All samples were prepared and analyzed in duplicate. The thousands of MS2 spectra from all time points were used to build a spectral network that allowed visualization of chemical species in both structurally familial and temporal contexts based on statistically significant similarities between their tandem MS fragmentation patterns (21, 30).

While NanoDESI affords unparalleled sampling, microbial MALDI-TOF IMS allows high-resolution mapping of ions within a sample (23). As a complement to the NanoDESI spectral networks, we also collected IMS data sets for each interaction and *S. coelicolor* control colonies at day five. The combined output from these complementary techniques provided a uniquely rich data set for simultaneously assessing the response of a single organism in multiple interactions at a system-wide scale and for prospecting for novel secondary metabolites.

**Interspecies interactions cause differential secondary metabolite production in *S. coelicolor*.** To broadly characterize the chemical response of *S. coelicolor* in these interactions, we considered these data in terms of chemical inputs from the initiator colonies and chemical output from *S. coelicolor*. In our work flow, we chose to represent the MS2 spectra visually via spectral networking, which allows each MS2 spectrum within the entire experimental data set to be compared in a pairwise manner to all other MS2 spectra and scored based on the statistical similarity between the two fragmentation patterns. When the results of this analysis are imported into two-dimensional (2D) visualization software (such as Cytoscape), this allows similar compounds to be grouped together in 2D space separate from other compounds

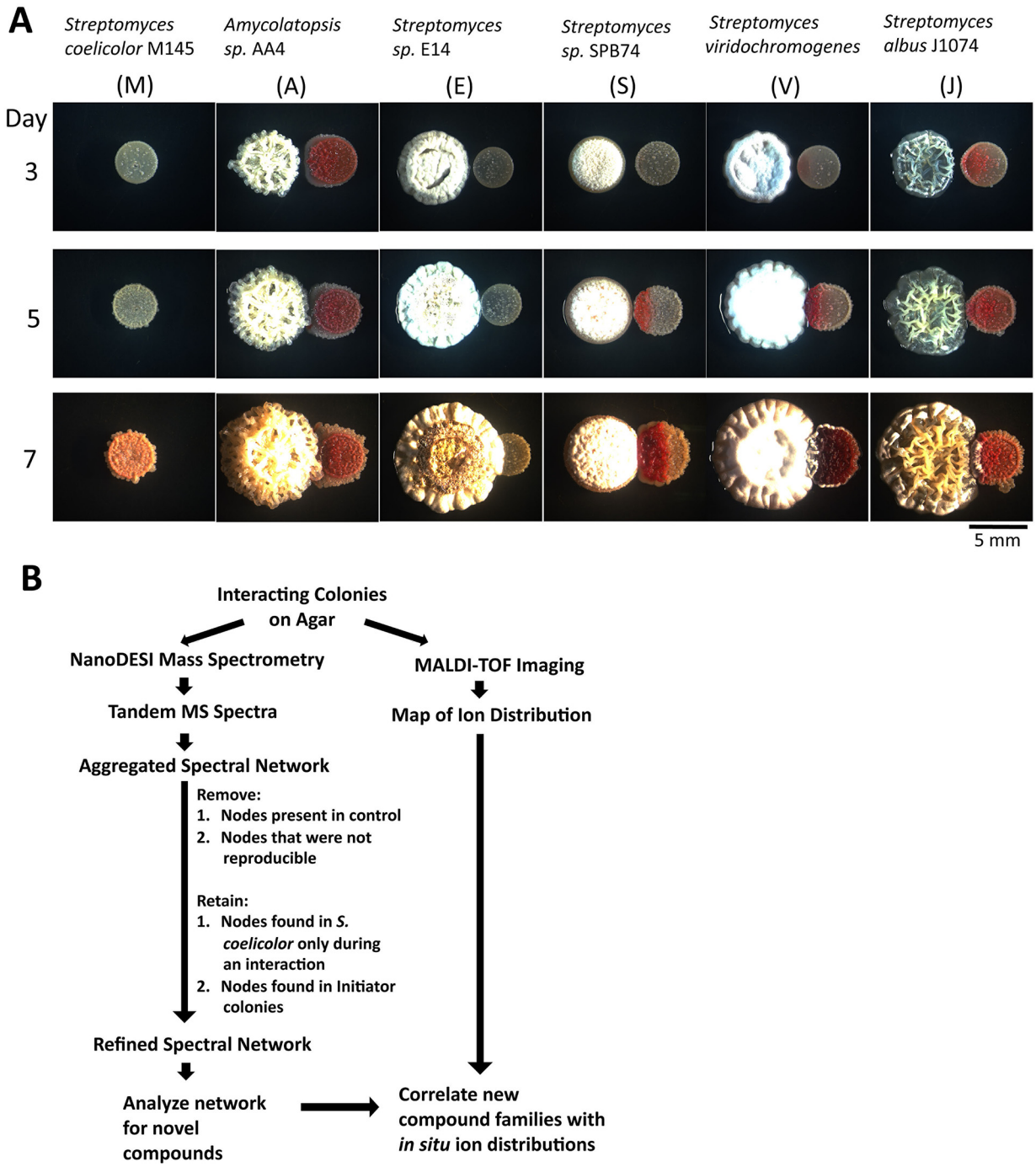


**FIG 1** *S. coelicolor* exhibits a variety of phenotypes in interactions with other actinomycetes. (A) Micrographs of colonies of *S. coelicolor* grown alone (first column) and near colonies of other actinomycetes. A range of *S. coelicolor* phenotypes, including differences in pigment production and multicellular development, is visible in interacting colonies over time. The labels M (*S. coelicolor* M145), A (*Amycolatopsis* sp. AA4), E (*Streptomyces* sp. E14), S (*Streptomyces* sp. SPB74), and V (*S. viridochromogenes* DSM 40736) are used throughout. (B) Methodological work flow. Each interaction was investigated using NanoDESI and MALDI-TOF imaging mass spectrometry. The resulting spectral networks and ion distributions form a comprehensive data set for analysis of these microbial interactions.

exhibiting different fragmentation patterns. In this visualization, individual compounds present in the samples are represented as single nodes (circles) within the spectral network (30), with each node containing one or many MS2 spectra, as is the case when multiple MS2 spectra are judged to be identical by the spectral scoring algorithms (31). When the MS2 spectra for two nodes meet a set of criteria designed to assess structural relatedness, they are connected with an edge (line) (21, 31). Applying this algorithm to the pooled data sets yielded an aggregated parent network, which was then filtered to maximize interpretability. This

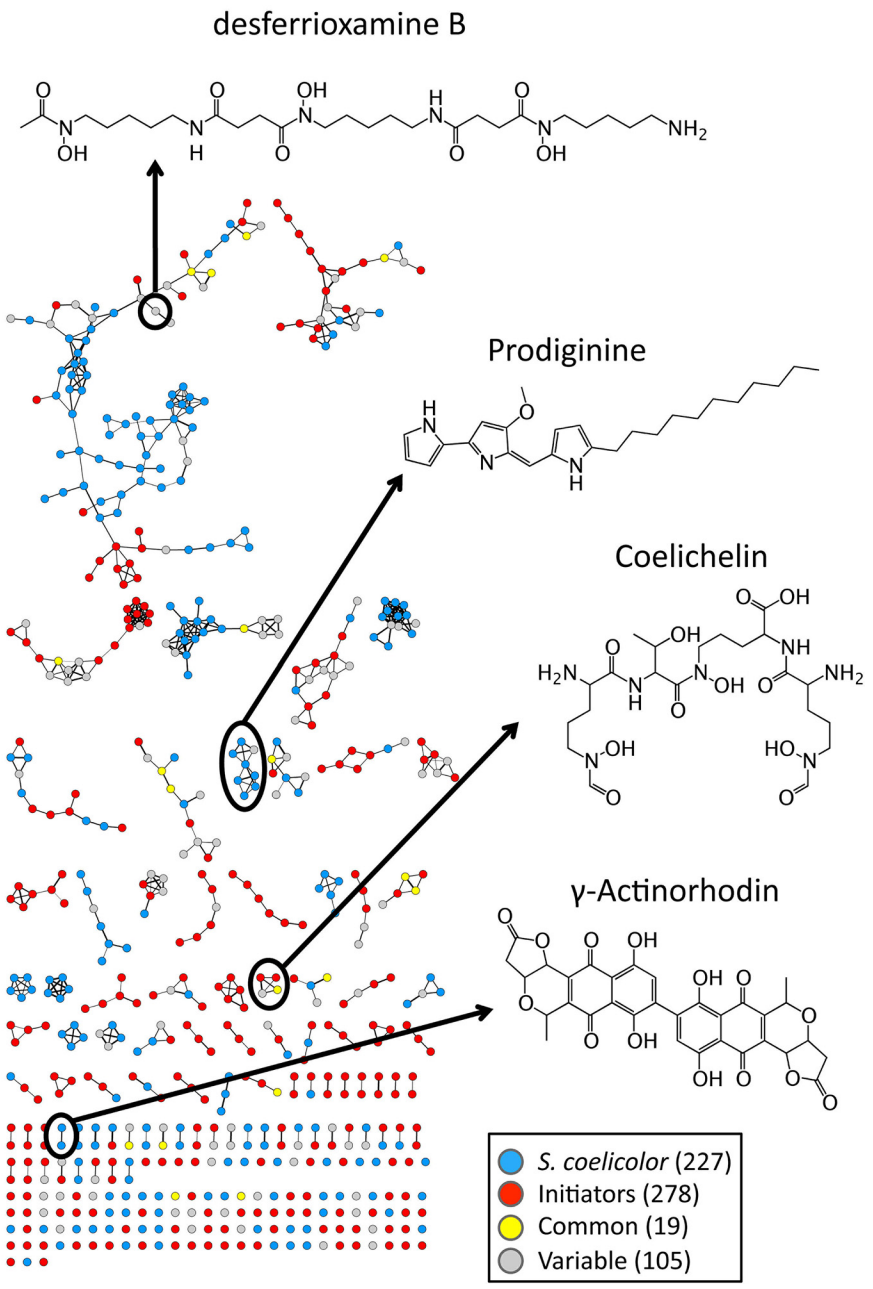


**FIG 2** Aggregated and refined spectral network of metabolites observed with NanoDESI during actinomycete interactions. The network is composed of nodes representing ions associated with *S. coelicolor* colonies grown near another actinomycete (ions found in *S. coelicolor* colonies grown alone were removed) and ions from initiator colonies. Nodes associated only with *S. coelicolor* at any time are blue. Nodes associated only with initiators are red. Nodes found only in both an initiator and *S. coelicolor* at the same time are yellow. Gray indicates nodes with variable behavior (i.e., found in multiple contexts). Representative structures of identified metabolites are shown.

entailed removing nodes associated with several controls, including the solvent alone, agar medium with no colonies, and *S. coelicolor* colonies grown alone at 3, 5, and 7 days. Finally, nodes were retained only if constituent spectra were found in both runs of data collection from duplicate samples, giving a refined network composed of nodes representing ions associated with the initiator colonies and *S. coelicolor* colonies during the interactions (Fig. 2).

The resulting network contains 629 total nodes. Of these, 227 nodes were associated exclusively with *S. coelicolor* colonies. There were 278 nodes associated exclusively with the various initiator colonies. Nineteen nodes were found only in both *S. coelicolor* and a given initiator at the same time (common), and 105 nodes showed variable behavior, i.e., they were found associated with *S. coelicolor* and/or an initiator at different times. Only 23 compounds were associated exclusively with *S. coelicolor* control colonies, and 43 compounds were common to interacting and control *S. coelicolor* colonies (see Fig. S25 in the supplementary appendix available at http://gasp.med.harvard.edu/journals/traxler_2013_SI_nanodesi.pdf). At a broad level, the spectral network shows that these interactions triggered production of many compounds by *S. coelicolor* which were not observed when *S. coelicolor* was grown in isolation.

To see how similar the response of *S. coelicolor* was between interactions, we constructed Venn diagrams encompassing all *S. coelicolor*-associated nodes for all five interactions for each day. The diagram for day three is shown in Fig. 3A. This analysis highlighted an important trend, namely that the majority of the nodes fall into the outer, or "unique," zones of the diagram, implying that they are interaction specific. For day three, the total number of unique nodes was 94, versus 29 that fell into the "shared" interior sections of the diagram. This trend was evident at every time point (Fig. 3B). We also note that while some interactions triggered production of relatively few compounds at a given time point (i.e., *S. albus* and *Streptomyces* sp. SPB74 at day 3), each interaction, with the exception of the *S. albus* interaction, underwent a time when the majority of its stimulated compounds were unique (see Venn analyses for days 5 and 7 in the supplemental appendix at the above URL). Taken together, these results suggest that the chemical response of *S. coelicolor* was highly idiosyncratic depending on the interacting strain and the time of sampling.

When we interrogated the network for known compounds in the *S. coelicolor* chemical response, we found subnetworks representing at least four major compound families: the antibiotics actinorhodin and prodiginine and the siderophores coelichelin and desferrioxamines B and E (Fig. 2). To examine the pattern of production of each of these molecular families, we considered the percentage of the total number of nodes for each family active in each interaction at each time point (heat map in Fig. 3C). For example, the prodiginine family of

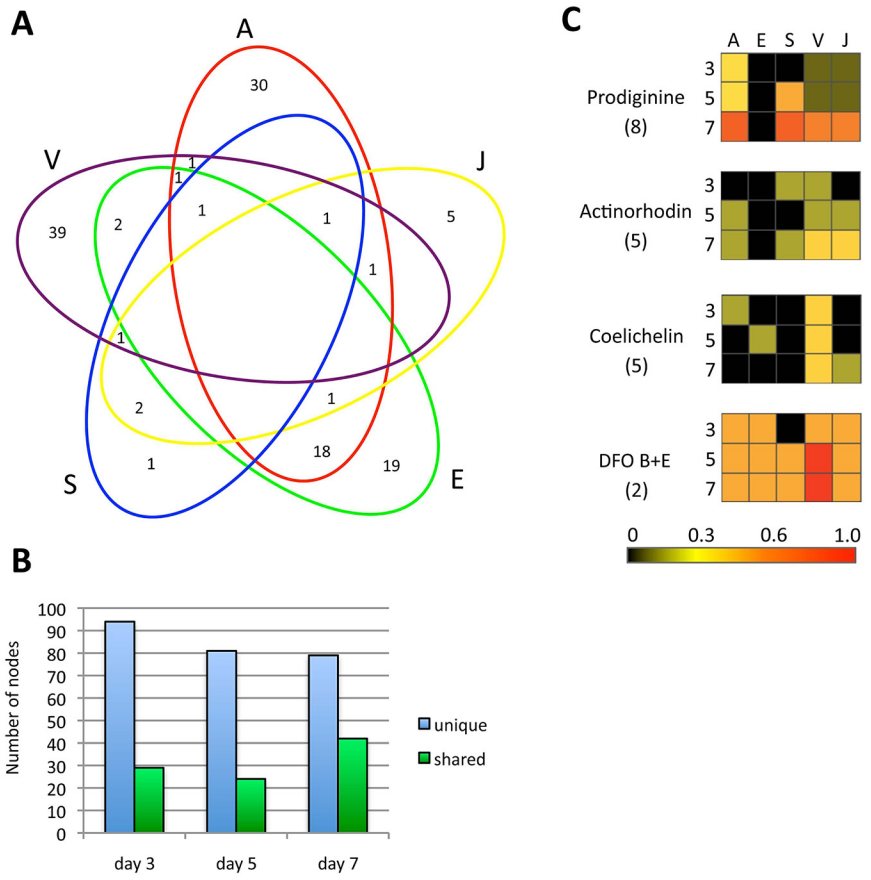


**FIG 3** Global analysis of metabolites observed with NanoDESI. (A) Venn analysis of nodes associated with interacting *S. coelicolor* colonies on day 3. Each ellipse contains nodes found in the indicated interaction. The majority of detected ions fall into the outer zones of the diagram, indicating that each interaction is more unique than it is similar to other interactions. (B) Numbers of unique and shared nodes found at each time point. For each day, the numbers of nodes found only in single interactions were summed to give the total number of unique nodes. Nodes that were found in more than one interaction were summed to find the total number of shared nodes. The number of unique nodes exceeds the number of shared nodes at every time point, suggesting that the response of *S. coelicolor* is different depending on the interaction. (C) Patterns of known compound production. Each compound family is observed as a subset of nodes within the larger network in Fig. 2. Heat map colors indicate the proportion of active nodes in each interaction. For example, 1.0 indicates that all the nodes associated with a given compound family are active. Three, 5, or 7 represents the sampling time in days. Numbers beneath compound names indicate number of nodes associated with those compounds in Fig. 2. Interactions are labeled as indicated in Fig. 1A. This analysis includes nodes associated with initiator colonies.

antibiotics is represented in the network as a subnetwork consisting of eight total nodes observed across all 5 interactions and all 3 time points. Six of these eight nodes were observed when *S. coelicolor* was interacting with *Amycolatopsis* sp. AA4 at day seven, representing robust stimulation of this compound family.

Production of each of these four compound families varied according to the interaction and sampling time. For example, *Streptomyces* sp. E14 did not stimulate prodiginine or actinorhodin production (as expected, given that no *S. coelicolor* pigmentation is evident in this interaction), while *Amycolatopsis* sp. AA4, *Streptomyces* sp. SPB74, *S. viridochromogenes*, and *S. albus* all stimulated production of both pigmented antibiotics, although the timing of production varied depending on the initiator. The genomes of all six strains examined in these interactions have been sequenced and analyzed for their secondary metabolic potential using the antiSMASH platform (32). The results of this analysis (provided in Table S5 in the supplemental appendix at http://gasp.med.harvard.edu/journals/traxler_2013_SI_nanodesi.pdf) showed that none of the initiator strains contains genes for production of either actinorhodin or prodiginines, and accordingly, all compounds of these families associated with these interactions are presumed to originate with *S. coelicolor*. As further validation of our overall approach, we determined the spatial distribution of the prodiginines within the interacting colonies using IMS (see Fig. S1 in the supplemental appendix at the above URL). Prodiginine distribution was found to match exactly the pattern expected given the visibility of red pigment and the activity of nodes within the prodiginine subnetwork.

Coelichelin was found sporadically across the interactions, with the exception of the *S. viridochromogenes* interaction, where it was observed at every time point. BLAST analysis of the *S. viridochromogenes* genome clearly shows that it too possesses the genes for coelichelin biosynthesis. Thus, observation of coelichelin in this interaction may reflect production by either or both of the strains. Desferrioxamine B or E was found in every interaction and at every time point with the exception of *Streptomyces* sp. SPB74 at day three. Genes for desferrioxamine production are widely distributed among actinomycetes, with *Streptomyces* sp. SPB74, *S. viridochromogenes*, and *S. albus* all containing canonical operons for biosynthesis of this siderophore. However, *Amycolatopsis* sp. AA4 and *Streptomyces* sp. E14 do not have desferrioxamine synthesis operons. Thus, in the *Amycolatopsis* sp. AA4 and *Streptomyces* sp. E14 interactions, the observed desferrioxamines likely originated from *S. coelicolor*, while either or both of the strains may be responsible for its production in the *Streptomyces sp.* SPB74, *S. viridochromogenes*, and *S. albus* interactions. The common detection of siderophores in these interactions suggests that competition for iron may be stringent in interactions between actinomycetes, a notion further underscored by our findings detailed below and previously observed under other interaction conditions (13).

**Extended family of acyl-desferrioxamines from *S. coelicolor*.** The spectral network in Fig. 2 contains many nodes of unknown identity associated with *S. coelicolor* colonies. A majority of these unknown nodes fall into four major subnetworks, highlighted in Fig. 4A. One of these subnetworks (a1) was indirectly connected to the node representing desferrioxamine B, leading us to consider that these compounds might be modified versions of desferriox-

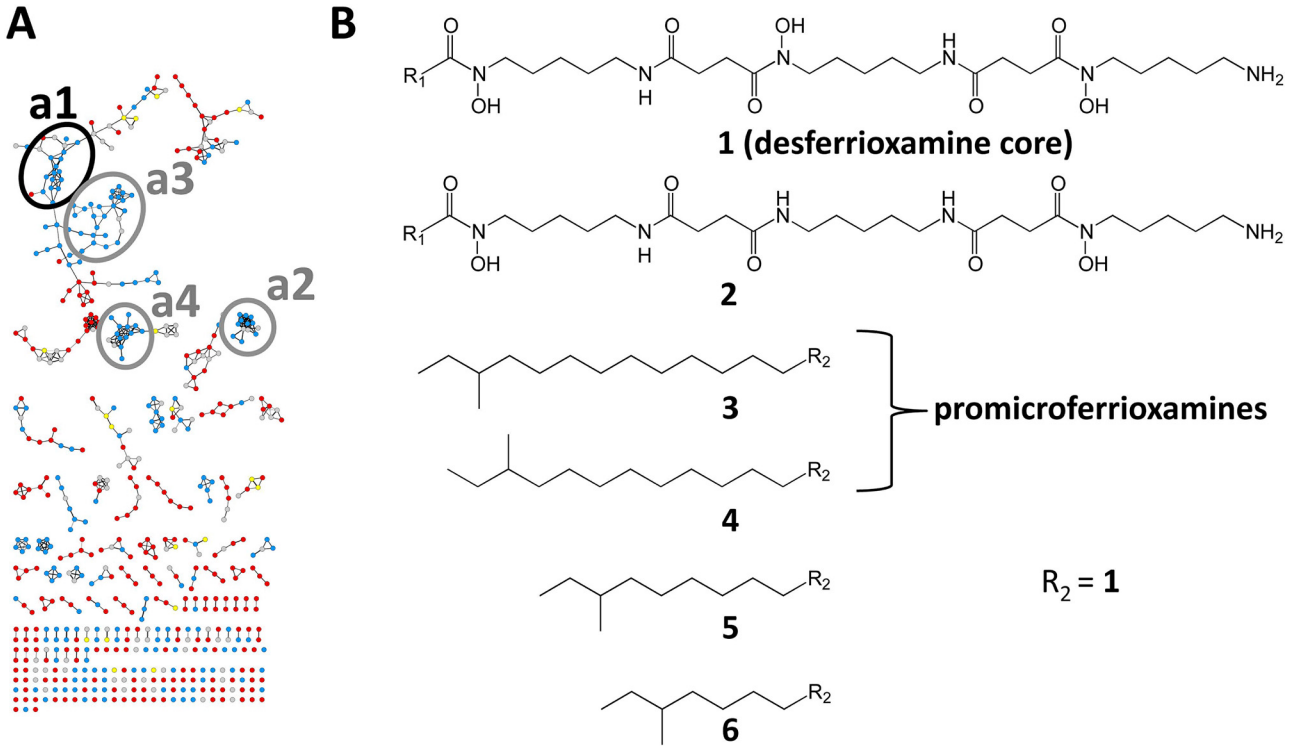


**FIG 4** Visualization of acyl-desferrioxamine (acyl-DFO) subnetworks and desferrioxamine structures. (A) Acyl-DFOs form four major subnetworks (numbered a1 to a4) within the larger spectral network. Subnetwork a1, circled in black, is magnified in Fig. 5. Subnetworks a2 to a4 are shown in Fig. S2 and S3 at http://gasp.med.harvard.edu/journals/traxler_2013_SI_nanodesi.pdf. (B) Structure 1 at the top constitutes the core desferrioxamine structure, while structure 2 lacks a complete central hydroxamate moiety. Structures 3 to 6 are acyl appendages from known acyl-desferrioxamines (11, 50). MS2 fragmentation patterns and *m*/*z* values from molecules bearing 3 to 6 match MS2 fragmentation patterns and *m*/*z* values found here to be made by *S. coelicolor*. The *m*/*z* values associated with each structure are 743 (structure 3), 729 (structure 4), 687 (structure 5), and 659 (structure 6).

amine. Confirming this possibility, we found that the MS2 spectra of four of the nodes in this subnetwork, representing compounds with *m*/*z* values of 743, 729, 687, and 659, matched exactly the MS2 spectra of several recently characterized acyl-desferrioxamines (33), including promicroferrioxamine (24). These molecules contain the core desferrioxamine siderophore structure (structure 1 in Fig. 4B) with a terminal R group composed of an acyl chain with an anteiso-methyl group (structures 3 to 6 in Fig. 4B). The fragmentation patterns for these known acyl-desferrioxamines provided the basis for annotation of more molecules in these subnetworks, ultimately showing that *S. coelicolor* made at least 12 analogs of the acyl-desferrioxamines, with appendages ranging from C7 to C17 fatty acids (summarized in Table S1 at http://gasp.med.harvard.edu/journals/traxler_2013_SI_nanodesi.pdf). We also observed a node with an *m*/*z* of 727 that corresponds to a previously described version of promicrodesferrioxamine with a nonhydroxylated central hydroxamate moiety (structure 2 in Fig. 4B).

Throughout the entire network, the nodes associated with these acyl-desferrioxamines total >90 and thus account for ~40% of the total response of *S. coelicolor* observable in the spectral network. Of the four major subnetworks circled in Fig. 4A, subnetworks a1 and a2 share broad redundancy in terms of the masses of their constituent nodes, although the discrete clustering of subnetwork a2 may indicate an unknown structural feature that sets these versions apart. Subnetwork a3 encompasses larger molecules that include versions of the $C_{12}$ and $C_{13}$ acyl-desferrioxamines with an unknown addition of ~118 Da (see Fig. S22 and S23 at the above URL). Finally, based on high-resolution masses, subnetwork a4 likely contains sodiated and potassiated adducts of the acyl-desferrioxamines (see Fig. S3 at the above URL). These findings show that *S. coelicolor* is capable of making an extensive repertoire of siderophores in the presence of other actinomycetes.

**Stimulation of acyl-desferrioxamine production in interspecies interactions.** Having deduced the identity of a key component of the *S. coelicolor* chemical response, we returned to the spectral network and IMS data to further examine the temporal and spatial pattern of acyl-desferrioxamine production across the five interactions. When the heat map analysis presented in Fig. 3C was extended to include 94 nodes representing the acyl-desferrioxamines, a clear pattern of production was apparent; namely, the *Amycolatopsis* sp. AA4 and *Streptomyces* sp. E14 interactions triggered robust acyl-desferrioxamine synthesis even at day 3 (Fig. 5A). In the case of the *Streptomyces* sp. E14 interaction, these molecules continued to be detected throughout the time course. In contrast, in the *Amycolatopsis* sp. AA4 interaction, the number of different acyl-desferrioxamine nodes was diminished on days five and seven, perhaps indicating uptake by the growing colony. Acyl-desferrioxamine production was observed starting at day 5 for the *Streptomyces* sp. SPB74 interaction and at day 7 for the *S. viridochromogenes* and *S. albus* interactions. These trends can be seen on a finer scale by examining the pattern of activity in different acyl-desferrioxamine subclusters within the spectral net-

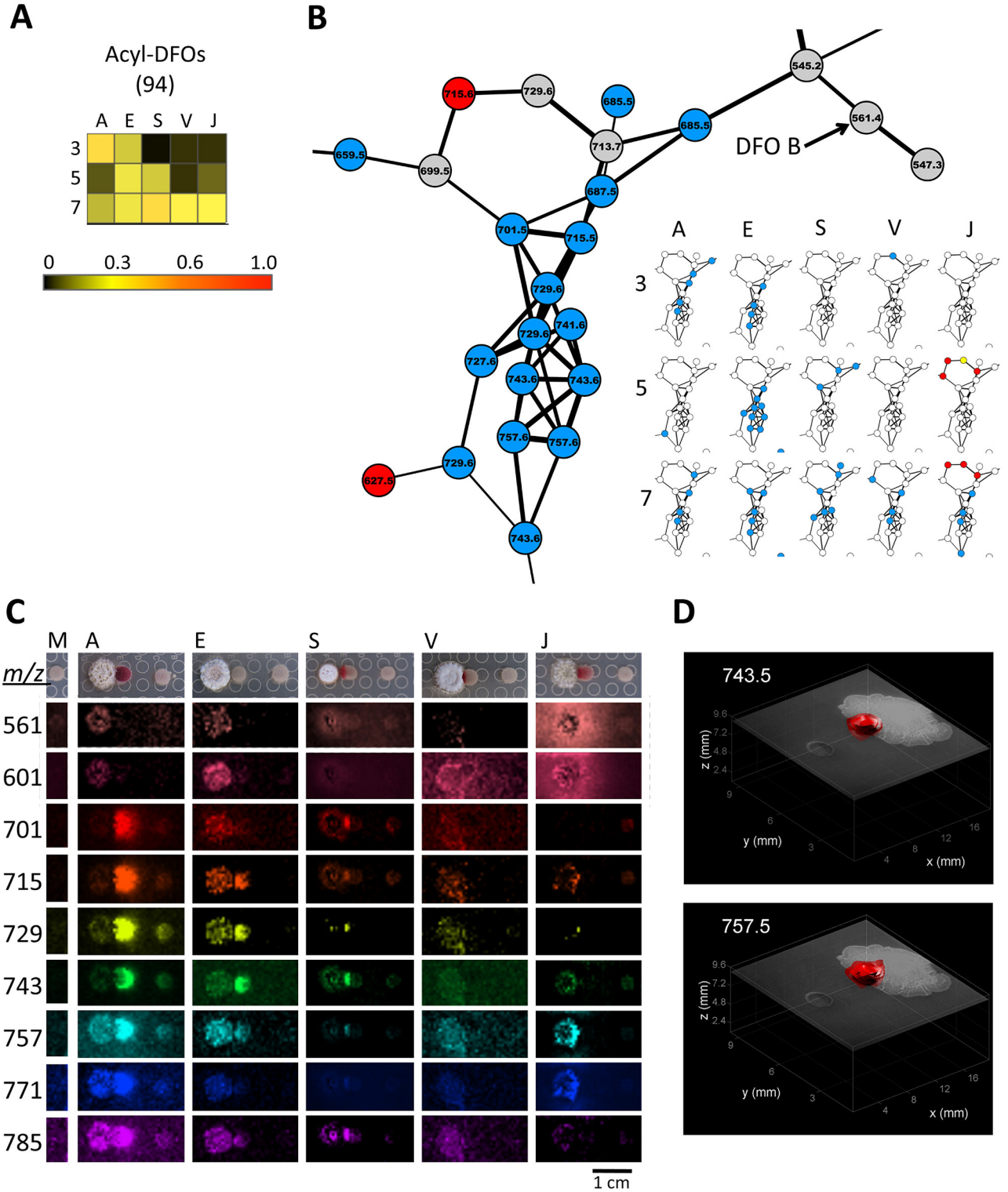


**FIG 5** Patterns of acyl-desferrioxamine production in interspecies interactions. (A) Heat map of acyl-desferrioxamine production. Analysis parameters are identical to those in Fig. 3C. (B) Subnetworks 1 and 2 contain the majority of acyl-desferrioxamines verified by MS2 fragmentation. Fine-scale analysis of subnetwork 1 is shown, illustrating differential acyl-desferrioxamine production in various interactions over time. Note the proximity of subnetwork 1 to desferrioxamine B (DFO B). Subnetworks 3 and 4 contain larger versions of DFOs and sodium adducts, respectively (see Fig. S3 at http://gasp.med.harvard.edu/journals/traxler_2013_SI_nanodesi.pdf). (C) Desferrioxamines are observable using IMS at day 5. *m/z* 561 and 601 correspond to desferrioxamines B and E, respectively. *m/z* 701 to 785 are representative acyl-desferrioxamines. Note the production of acyl-desferrioxamines by *S. coelicolor* in interactions where initiator strains do not make desferrioxamines B and/or E. Each IMS signal is scaled as a single color heat map; brighter color indicates higher signal intensity, and darker indicates lower signal intensity. (D) Acyl-desferrioxamines diffuse away from *S. coelicolor* colonies in three dimensions. The outermost to innermost layers (isosurfaces) correspond to 0.8, 0.88, and 0.95% ion intensity.

work, including subnetwork a1, shown in Fig. 5B. Activity in subnetworks a2 to -4 also mirrors this pattern (see the supplemental appendix at http://gasp.med.harvard.edu/journals/traxler_2013_SI_nanodesi.pdf).

We also examined the distribution of acyl-desferrioxamine production using IMS at day 5 (Fig. 5C). To serve as an internal control for the IMS experiments, an additional *S. coelicolor* colony was spotted 1 cm away from the *S. coelicolor* colony that was directly adjacent to the initiator colony. A subset of the acyl-desferrioxamines with *m*/*z* values ranging from 701 to 785 was readily detectable using this technique. Consistent with the activity within the NanoDESI spectral network, we saw production of the acyl-desferrioxamines in the *Amycolatopsis* sp. AA4, *Streptomyces* sp. E14, and *Streptomyces* sp. SPB74 interactions. Little to no acyl-desferrioxamine production was seen in the *S. viridochromogenes* and *S. albus* interactions; however, desferrioxamine E (*m*/*z* 601) was produced by both of the initiator strains. *S. albus* produced a large amount of deferrioxamine B as well (*m*/*z* 561). The near colonies in the *Amycolatopsis* sp. AA4 and *Streptomyces* sp. E14 interactions showed the most acyl-desferrioxamine production, with molecules even being detected beyond the border of the colony in several cases in the *Amycolatopsis* sp. AA4 interaction. To further examine the distribution of the acyl-desferrioxamines, we used a newly developed three-dimensional (3D) MALDI-TOF IMS methodology (34) (Fig. 5D). The resulting 3D renderings show that the representative acyl-desferrioxamines at *m*/*z* 743 and 757 were distributed beyond the edge of the colony not only on the agar surface but below the producing colony as well. Overall, these data imply that while the temporality and amount of acyl-desferrioxamine production varied among the interactions, all of the interactions eventually led to competition for iron. Moreover, the acyl-desferrioxamines were especially abundant in the interactions with the two strains that likely utilize siderophores other than desferrioxamine for iron acquisition (i.e., *Amycolatopsis* sp. AA4 and *Streptomyces* sp. E14).

**Siderophores from other strains trigger acyl-desferrioxamine production in *S. coelicolor*.** The apparent competition for iron induced in these interactions prompts the hypothesis that siderophores from initiator strains might locally decrease the iron available to *S. coelicolor* and thus stimulate acyl-desferrioxamine synthesis. Our previous work with *Amycolatopsis* sp. AA4 showed that it makes a unique siderophore, amychelin, which cannot be used by *S. coelicolor* (12, 13). Several amychelin adducts were observed in the spectral network as a subnetwork associated with the *Amycolatopsis* sp. AA4 interaction (Fig. 6A, listed in Table S3 at http://gasp.med.harvard.edu/journals/traxler_2013_SI_nanodesi.pdf). *Amycolatopsis* sp. AA4 strains with mutations in the *amcG* locus are unable to make amychelin (13). To determine if amychelin might play a role in activating acyl-desferrioxamine synthesis in *S. coelicolor*, we grew a colony of the *Amycolatopsis* sp. AA4 Δ*amcG* strain adjacent to *S. coelicolor* and examined molecule production using IMS. Production of four representative ions from the acyl-desferrioxamine family are shown in Fig. 6B in interactions with both wild-type *Amycolatopsis sp.* AA4 and the Δ*amcG* strain. Much less acyl-desferrioxamine, both in area and in abundance, was produced by *S. coelicolor* in the interaction with the Δ*amcG* strain than in the wild-type *Amycolatopsis* sp. AA4 interaction. To further examine if iron starvation alone could trigger production of the acyl-desferrioxamines, we tested the ability of the iron chelator 2,2′-dipyridyl to stimulate production of these molecules (see Fig. S26 in the supplementary appendix at the above URL). Indeed, we found that when 2,2′-dipyridyl was included at 200 μM, acyl-desferrioxamines were produced. These results confirm that iron competition caused by xenosiderophores can lead to induction of acyl-desferrioxamine biosynthesis in *S. coelicolor* and that iron starvation alone is sufficient to trigger production of these siderophores.

## DISCUSSION

In natural environments, such as the soil, bacteria live surrounded by a multitude of other organisms, including other bacteria. Actinomycetes, whose genomes contain numerous gene clusters for making complex secreted metabolites, have clearly evolved many and diverse chemical means to affect other nearby residents of the soil (3, 5). Humans have long been the beneficiaries of this evolutionary process, since the majority of natural products used clinically originate with actinomycete bacteria (1, 2). However, how actinomycetes deploy their arsenals of secondary metabolites in the presence of other species has remained largely mysterious.

In this work, we used two mass spectrometry techniques, NanoDESI and MALDI-TOF imaging, to profile the chemical output from the actinomycete *S. coelicolor* in interactions with five other species of actinomycetes. Importantly, these complementary techniques allowed interrogation of the secreted metabolites directly from the bacterial colonies. The resulting data sets comprise the most comprehensive chemical view of a related set of microbial interactions to date. The spectral network yielded by our analyses includes some 629 compounds. Importantly, many of these molecules are of unknown identity. Surprisingly, we found that the set of compounds associated with *S. coelicolor* colonies varied dramatically from interaction to interaction, suggesting a largely specific response in each case (Fig. 3). Several interactions triggered production of an extended family of acyl-desferrioxamine siderophores, never before observed from *S. coelicolor* (Fig. 4). This result illustrates that interspecies interactions can lead to unexpected biosynthetic shifts in secondary metabolic pathways. Together, these findings indicate that during interspecies interactions, the chemical landscape exploited by actinomycetes is both vast and dynamic. Moreover, the great number of unidentified metabolites present in these data sets hints that interspecies interactions may represent a new path to accessing the rich chemical diversity encoded in actinomycete genomes.

*S. coelicolor* produces several compounds representative of therapeutically important chemical families. These include desferrioxamines (used to treat iron toxicity [35]), prodiginines (currently being investigated as immunosuppressant anticancer agents [36, 37]), and the calcium-dependent antibiotic (similar to the drug daptomycin [38]). Here, we observed a large number (227) of compounds differentially associated with *S. coelicolor* colonies across the five interactions. Of these, 50% (114) are readily classified as related to known *S. coelicolor* metabolites, including the prodiginines, actinorhodins, coelichelins, and the newly observed acyl-desferrioxamines. *S. coelicolor* has many other gene clusters for uncharacterized metabolites (25), some of which likely account for the many unknown compounds we detected. It is also possible that some of the compounds found exclusively associated with *S. coelicolor* colonies may have had precursors made by the initiator colonies that were later modified directly or indirectly by *S. coelicolor*. NanoDESI and IMS analyses of *S. coelicolor* strains

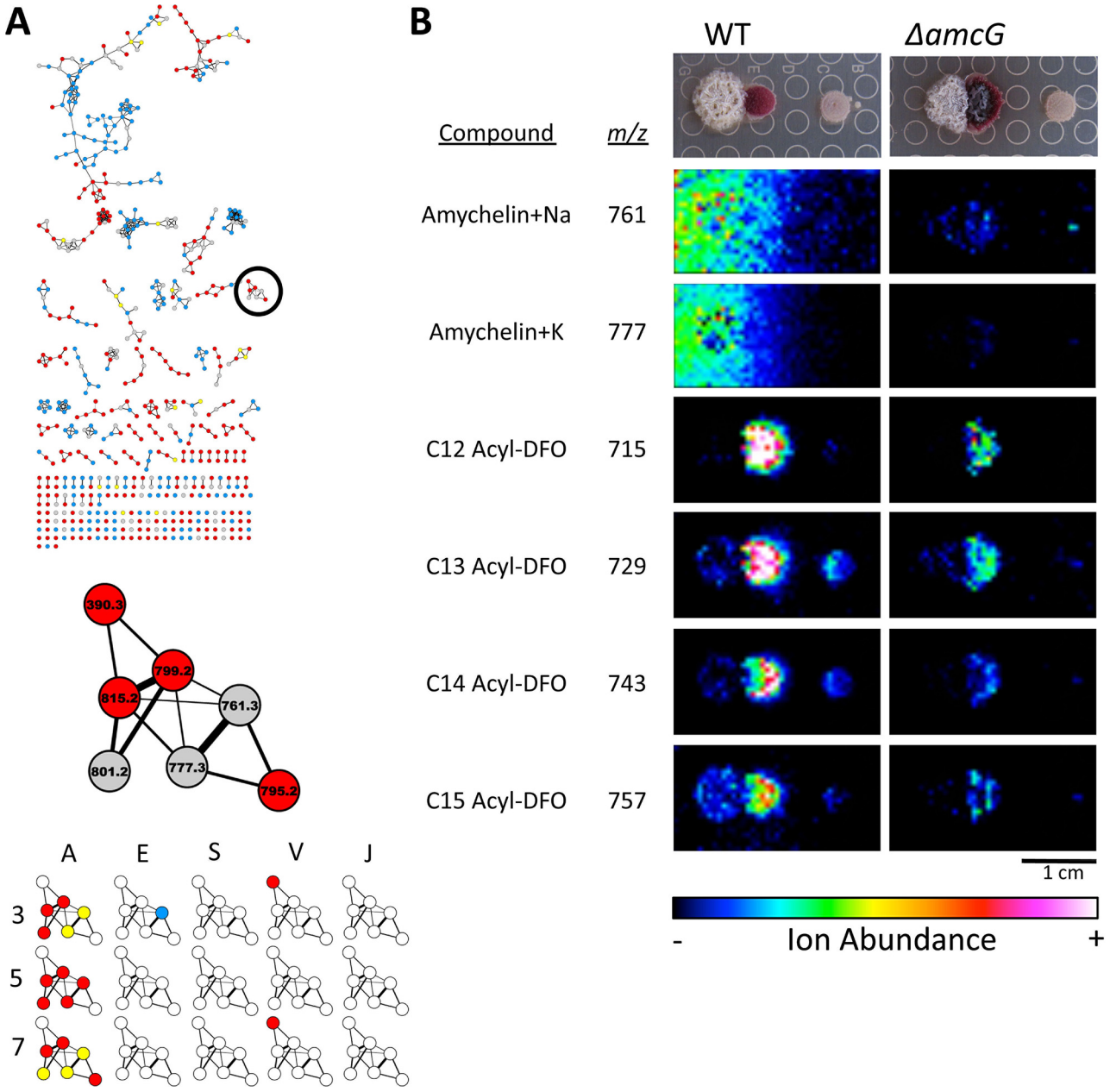


**FIG 6** Acyl-desferrioxamine production by *S. coelicolor* is stimulated by a siderophore from a nearby actinomycete. (A) The actinomycete *Amycolatopsis* sp. AA4 produces the siderophore amychelin. Sodiated and potassiated adducts of amychelin are visible as an *Amycolatopsis* sp. AA4-associated subnetwork. (B) Five days IMS of *S. coelicolor* grown near wild-type *Amycolatopsis* sp. AA4 and a mutant lacking the gene *amcG*, which does not produce amychelin. Ion abundance is visualized as a heat map. When grown near the Δ*amcG* strain, which does not make amychelin, *S. coelicolor* produces much less of the acyl-desferrioxamines.

with mutations in various gene clusters will be required to positively link the many unidentified compounds observed here with specific genes. As such, our current work sets the stage and provides a solid foundation for future studies to characterize the currently cryptic secondary metabolome of this streptomycete and many others like it.

The family of desferrioxamines described here has fatty acid appendages ranging from 7 to 17 carbon units. While several acyl-desferrioxamine versions have been found from at least two bacterial species (24, 33), the range of the acyl-desferrioxamines produced by *S. coelicolor* is unprecedented. Interestingly, both the promicroferrioxamines and the other known examples of acyl-desferrioxamines were isolated from actinobacteria sampled from intertidal habitats, initially suggesting that desferrioxamine acylation might be an adaptation to life in marine environments (24, 33). Further reinforcing this notion, marine bacteria from diverse genera are known to produce suites of acylated siderophores (39), including the marinobactins (40), aquachelins (40), amphibactins (41), ochrobactins (42), and synechobactins (43). While a few other acylated siderophores are known from terrestrial bacteria (44–46), the finding that *S. coelicolor* makes a very large suite of acylated desferrioxamines strongly suggests that the advantages

associated with modulating siderophore solubility are not limited to marine environments.

Siderophores with relatively long fatty acid tails, such as mycobactin T and the amphibactins (14 to 21 carbons in length), have been found associated with cell membranes (41, 47), while siderophores such as marinobactins and aquachelins, with 12 to 16 carbons in their acyl chains, are known to partition as micelles and vesicles into the aqueous environment (40). Other siderophores, with acyl chain lengths of 10 carbons or less, such as rhizobactins and carboxymycobactins, diffuse relatively freely (39, 47). Moreover, synthetic acylation of desferrioxamine B, with appendages of up to 7 carbons in length, was shown to alter their solubility and membrane permeability (48). The range of acyl moieties found in the *S. coelicolor* desferrioxamines, from a single carbon in desferrioxamine B, 3 carbons in desferrioxamines E and G, and 7 to 17 carbons for the new versions found here, encompasses the entire range of solubility. We note that versions of desferrioxamines with appendages ranging from C11 to C14 were clearly present beyond the edges and below *S. coelicolor* colonies (Fig. 5C and D, *Amycolatopsis* sp. AA4 interaction), possibly hinting that micelle-mediated iron acquisition may be occurring here. We also observed that production of the acyl-desferrioxamines was largely stimulated by production of a competing siderophore by one of the initiator strains (Fig. 6). Together, these findings point to a remarkably diversified foraging strategy in the face of fierce competition for iron.

The biosynthetic pathway for desferrioxamine is well documented (49, 50). The third step of the proposed pathway entails the acylation of *N*-hydroxycadaverine by the enzyme DesC to yield *N*-hydroxy-*N*-succinyl-1,5-diaminopentane (hsDAP), three units of which then serve as building blocks for the final trimeric desferrioxamine structure. In organisms that make desferrioxamines B and G (including *S. coelicolor*), DesC is proposed to have relaxed substrate specificity, allowing it to incorporate acetyl-coenzyme A (CoA) or succinyl-CoA into desferrioxamine precursors (50). The acyl moieties found in place of the normal acetyl-CoA or succinyl-CoA additions suggest that the relaxed substrate specificity of *S. coelicolor* DesC may extend much further than originally thought, allowing it to incorporate these long acyl chains into the normal desferrioxamine biosynthetic pathway.

The experimental framework utilized here yields data sets that afford unique opportunities for the discovery of natural products. Indeed, the differential chemical output observed from *S. coelicolor* implies that this bacterium has great flexibility in the expression of its secondary metabolome. While competition for iron provides a straightforward rationale for the induction of siderophore synthesis in *S. coelicolor* interactions with other actinomycetes, the physiological cues underlying the induction of antibiotics and other metabolites remain to be elucidated. Understanding the mechanisms of such interactions is of great interest since they may offer a new door to accessing "cryptic" metabolites from other actinomycetes.

An appendix containing supplemental figures and chemical annotations for the molecules detected in this study can be accessed at http://gasp.med.harvard.edu/journals/traxler_2013_SI_nanodesi.pdf.

## MATERIALS AND METHODS

**Strains and growth conditions.** Strains used in this study are listed in Table S4 in the supplemental appendix at http://gasp.med.harvard.edu/journals/traxler_2013_SI_nanodesi.pdf. All experiments were done on ISP2 agar (10 g malt extract, 4 g glucose, 4 g yeast extract, 15 g agar, 1 liter Milli-Q $H_2O$). For all experiments, 10 ml of agar was added to standard 100-mm petri plates to yield an agar surface ~2 mm thick, which is suitable for preparation for IMS. Strains were inoculated onto agar in 1-$\mu$l aliquots from frozen spore suspensions. *S. coelicolor* and the initiator strains were spotted 5 mm apart at the same time. For IMS experiments, a second colony of *S. coelicolor* was spotted 1 cm away from the first *S. coelicolor* colony to serve as an internal control. Petri plates were incubated at 30°C until the appropriate time points in large sealable bags to prevent desiccation.

**MALDI-TOF imaging mass spectrometry.** IMS was carried out as described previously (22, 24). At the appropriate time point, colonies and the surrounding agar were cut and removed from petri plates and transferred to Bruker MSP 96 anchor plates. The samples were then sprinkled with Universal MALDI Matrix (Fluka 50149) using a 53-$\mu$m sieve. Once a thick, uniform layer of matrix was deposited on the sample, it was placed at 37°C for 4 h or until it was completely desiccated. Excess matrix was blown off with compressed air, and any residue remaining on exposed surfaces of the MALDI plate was wiped away with methanol. Spectra were acquired using a Bruker Autoflex MALDI-TOF MS, and ions were visualized using Fleximaging software. 3D IMS was performed as described previously (34). Briefly, an 8-mm-thick section of agar was excised and cut widthwise at room temperature using microtome blades into 1.0-mm sections with each section placed on its side on the MALDI plate. 2D MALDI-TOF IMS analysis was conducted. Then, data were imported in the Matlab software program, where sections were aligned and processing was performed. The resulting 3D volume data set corresponding to an *m*/*z* value was visualized using 50%, 75%, and 90% semitransparent isosurfaces, indicating 80%, 88%, and 95% relative abundances of the molecular compound within the imaging area, respectively.

**NanoDESI mass spectrometry.** NanoDESI mass spectrometry was carried out essentially as described elsewhere (21). The NanoDESI source was coupled to a Thermo LTQ-FT-ICR (linear trap quadrupole Fourier transform ion cyclotron resonance) MS. Briefly, at the desired time points, samples were placed on the NanoDESI sample stage, and the liquid bridge was placed in contact with the sample for 15 min. During this time, the liquid bridge was placed at several locations on the colonies themselves and on the agar adjacent to the colonies located on the opposite side from the interacting strain. All data were collected in the positive ion mode in the range of 100 to 2,000 *m*/*z* using a solvent consisting of 65% acetonitrile and 35% water containing 0.05% formic acid. The data acquisition mode excluded ions for 10 min once they had been trapped and fragmented three times.

**Computation of mass spectral networks.** Spectral networks were assembled largely as described elsewhere (21). MS2 spectra were clustered using the MS-Clustering software program to build consensus spectra for repeatedly observed ions (31). Pairs of consensus spectra were aligned if both spectra fell within the top 10 alignments for each of the respective spectra and the cosine of their peak match scores was $\geq$0.6. The algorithms assumed a peak mass tolerance of 1.0 Da and an MS2 peak tolerance of 0.5 Da. The networks were visualized in the software program Cytoscape (51), where consensus spectra are represented as nodes connected by edges to aligning nodes. In order to maximize chemical/biological interpretability, nodes found in several control data sets were removed. These included nodes found associated with the solvent, the agar substrate, and *S. coelicolor* colonies grown in isolation at 3, 5, and 7 days. Finally, only nodes that were reproducible in both runs of data collection were retained.

## ACKNOWLEDGMENTS

We gratefully acknowledge Elizabeth Shank for making strains available and Mohammad Seyedsayamdost for helpful analytical discussions.

This work was supported by the National Institutes of Health (grant GM82137 to R.K. and postdoctoral fellowship 5F32GM089044-02 to M.F.T.). Work in this area in the P.C.D. laboratory for the development of

real-time MS was supported by National Institutes of Health (NIH) grant GM094802; work on interspecies interactions was supported by NIH grant AI095125. T.A. and P.C.D. also acknowledge financial support from the European Union 7th Framework Programme (grant 305259).

## ADDENDUM IN PROOF

While this manuscript was in review, another paper appeared that also observed the production of acylated desferrioxamines from *S. coelicolor* (A. M. Sidebottom, A. R. Johnson, J. A. Karty, D. J. Trader, and E. E. Carlson. ACS Chem Biol. 2013, doi:10.1021/cb4002798).

## REFERENCES


1. **Baltz RH.** 2008. Renaissance in antibacterial discovery from actinomycetes. Curr. Opin. Pharmacol. **8:**557–563.
2. **Bérdy J.** 2005. Bioactive microbial metabolites. J. Antibiot. Tokyo **58:** 1–26.
3. **Clardy J, Fischbach MA, Currie CR.** 2009. The natural history of antibiotics. Curr. Biol. **19:**R437–R441. doi: 10.1016/j.cub.2009.04.001.
4. **Fischbach MA, Walsh CT.** 2009. Antibiotics for emerging pathogens. Science **325:**1089–1093.
5. **Challis GL, Hopwood DA.** 2003. Synergy and contingency as driving forces for the evolution of multiple secondary metabolite production by Streptomyces species. Proc. Natl. Acad. Sci. U. S. A. **100**(Suppl 2): 14555–14561.
6. **Fischbach MA.** 2009. Antibiotics from microbes: converging to kill. Curr. Opin. Microbiol. **12:**520–527.
7. **O'Brien J, Wright GD.** 2011. An ecological perspective of microbial secondary metabolism. Curr. Opin. Biotechnol. **22:**552–558.
8. **Davies J.** 2007. Small molecules: the lexicon of biodiversity. J. Biotechnol. **129:**3–5.
9. **Romero D, Traxler MF, López D, Kolter R.** 2011. Antibiotics as signal molecules. Chem. Rev. **111:**5492–5505.
10. **Ueda K, Kawai S, Ogawa H, Kiyama A, Kubota T, Kawanobe H, Beppu T.** 2000. Wide distribution of interspecific stimulatory events on antibiotic production and sporulation among Streptomyces species. J. Antibiot. (Tokyo) **53:**979–982.
11. **Yamanaka K, Oikawa H, Ogawa HO, Hosono K, Shinmachi F, Takano H, Sakuda S, Beppu T, Ueda K.** 2005. Desferrioxamine E produced by Streptomyces griseus stimulates growth and development of Streptomyces tanashiensis. Microbiology **151:**2899–2905.
12. **Seyedsayamdost MR, Traxler MF, Zheng SL, Kolter R, Clardy J.** 2011. Structure and biosynthesis of Amychelin, an unusual mixed-ligand siderophore from Amycolatopsis sp. AA4. J. Am. Chem. Soc. **133:** 11434–11437.
13. **Traxler MF, Seyedsayamdost MR, Clardy J, Kolter R.** 2012. Interspecies modulation of bacterial development through iron competition and siderophore piracy. Mol. Microbiol. **86:**628–644.
14. **Vetsigian K, Jajoo R, Kishony R.** 2011. Structure and evolution of Streptomyces interaction networks in soil and in silico. PLoS Biol. **9:**e1001184. http://dx.doi.org/doi:10.1371/journal.pbio.1001184.
15. **Hoefler BC, Gorzelnik KV, Yang JY, Hendricks N, Dorrestein PC, Straight PD.** 2012. Enzymatic resistance to the lipopeptide surfactin as identified through imaging mass spectrometry of bacterial competition. Proc. Natl. Acad. Sci. U. S. A. **109:**13082–13087.
16. **Luti KJ, Mavituna F.** 2011. Elicitation of Streptomyces coelicolor with dead cells of Bacillus subtilis and Staphylococcus aureus in a bioreactor increases production of undecylprodigiosin. Appl. Microbiol. Biotechnol. **90:**461–466.
17. **Luti KJ, Mavituna F.** 2011. Streptomyces coelicolor increases the production of undecylprodigiosin when interacted with Bacillus subtilis. Biotechnol. Lett. **33:**113–118.
18. **Schneider J, Yepes A, Garcia-Betancur JC, Westedt I, Mielich B, López D.** 2012. Streptomycin-induced expression in Bacillus subtilis of YtnP, a lactonase-homologous protein that inhibits development and streptomycin production in Streptomyces griseus. Appl. Environ. Microbiol. **78:** 599–603.
19. **Straight PD, Fischbach MA, Walsh CT, Rudner DZ, Kolter R.** 2007. A singular enzymatic megacomplex from Bacillus subtilis. Proc. Natl. Acad. Sci. U. S. A. **104:**305–310.
20. **Straight PD, Willey JM, Kolter R.** 2006. Interactions between Streptomyces coelicolor and Bacillus subtilis: role of surfactants in raising aerial structures. J. Bacteriol. **188:**4918–4925.
21. **Watrous J, Roach P, Alexandrov T, Heath BS, Yang JY, Kersten RD, van der Voort M, Pogliano K, Gross H, Raaijmakers JM, Moore BS, Laskin J, Bandeira N, Dorrestein PC.** 2012. Mass spectral molecular networking of living microbial colonies. Proc. Natl. Acad. Sci. U. S. A. **109:**E1743–E1752. doi: 10.1073/pnas.1113306109.
22. **Yang YL, Xu Y, Straight P, Dorrestein PC.** 2009. Translating metabolic exchange with imaging mass spectrometry. Nat. Chem. Biol. **5:**885–887.
23. **Watrous JD, Dorrestein PC.** 2011. Imaging mass spectrometry in microbiology. Nat. Rev. Microbiol. **9:**683–694.
24. **Yang YL, Xu Y, Kersten RD, Liu WT, Meehan MJ, Moore BS, Bandeira N, Dorrestein PC.** 2011. Connecting chemotypes and phenotypes of cultured marine microbial assemblages by imaging mass spectrometry. Angew. Chem. Int. Ed. Engl. **50:**5839–5842.
25. **Bentley SD, Chater KF, Cerdeno-Tarraga AM, Challis GL, Thomson NR, James KD, Harris DE, Quail MA, Kieser H, Harper D, Bateman A, Brown S, Chandra G, Chen CW, Collins M, Cronin A, Fraser A, Goble A, Hidalgo J, Hornsby T, Howarth S, Huang CH, Kieser T, Larke L, Murphy L, Oliver K, O'Neil S, Rabbinowitsch E, Rajandream MA, Rutherford K, Rutter S, Seeger K, Saunders D, Sharp S, Squares R, Squares S, Taylor K, Warren T, Wietzorrek A, Woodward J, Barrell BG, Parkhill J, Hopwood DA.** 2002. Complete genome sequence of the model actinomycete Streptomyces coelicolor A3. Nature **417:**-141–147.
26. **Flärdh K, Buttner MJ.** 2009. Streptomyces morphogenetics: dissecting differentiation in a filamentous bacterium. Nat. Rev. Microbiol. **7:**36–49.
27. **McCormick JR, Flärdh K.** 2012. Signals and regulators that govern Streptomyces development. FEMS Microbiol. Rev. **36:**206–231.
28. **Willey JM, Gaskell AA.** 2011. Morphogenetic signaling molecules of the streptomycetes. Chem. Rev. **111:**174–187.
29. **Kieser T, Bibb M, Buttner M, Chater K, Hopwood D.** 2000. Practical Streptomyces genetics. John Innes Foundation, Norwich, CT.
30. **Guthals A, Watrous JD, Dorrestein PC, Bandeira N.** 2012. The spectral networks paradigm in high throughput mass spectrometry. Mol. Biosyst. **8:**2535–2544.
31. **Frank AM, Bandeira N, Shen Z, Tanner S, Briggs SP, Smith RD, Pevzner PA.** 2008. Clustering millions of tandem mass spectra. J. Proteome Res. **7:**113–122.
32. **Blin K, Medema MH, Kazempour D, Fischbach MA, Breitling R, Takano E, Weber T.** 2013. antiSMASH 2.0—a versatile platform for genome mining of secondary metabolite producers. Nucleic Acids Res. **41:**W204–W212. doi: 10.1093/nar/gkt449.
33. **D'Onofrio A, Crawford JM, Stewart EJ, Witt K, Gavrish E, Epstein S, Clardy J, Lewis K.** 2010. Siderophores from neighboring organisms promote the growth of uncultured bacteria. Chem. Biol. **17:**254–264.
34. **Watrous JD, Phelan VV, Hsu CC, Moree WJ, Duggan BM, Alexandrov T, Dorrestein PC.** 2013. Microbial metabolic exchange in 3D. ISME J. **7:**770–780.
35. **Kwiatkowski JL.** 2011. Real-world use of iron chelators. Hematol. Am. Soc. Hematol. Educ. Prog. 2011:451–458.
36. **Pandey R, Chander R, Sainis KB.** 2009. Prodigiosins as anti cancer agents: living up to their name. Curr. Pharm. Des. **15:**732–741.
37. **Pandey R, Chander R, Sainis KB.** 2007. Prodigiosins: a novel family of immunosuppressants with anti-cancer activity. Indian J. Biochem. Biophys. **44:**295–302.
38. **Baltz RH, Miao V, Wrigley SK.** 2005. Natural products to drugs: daptomycin and related lipopeptide antibiotics. Nat. Prod. Rep. **22:**717–741.
39. **Butler A.** 2005. Marine siderophores and microbial iron mobilization. Biometals **18:**369–374.
40. **Martinez JS, Zhang GP, Holt PD, Jung HT, Carrano CJ, Haygood MG, Butler A.** 2000. Self-assembling amphiphilic siderophores from marine bacteria. Science **287:**1245–1247.
41. **Martinez JS, Carter-Franklin JN, Mann EL, Martin JD, Haygood MG, Butler A.** 2003. Structure and membrane affinity of a suite of amphiphilic siderophores produced by a marine bacterium. Proc. Natl. Acad. Sci. U. S. A. **100:**3754–3759.
42. **Martin JD, Ito Y, Homann VV, Haygood MG, Butler A.** 2006. Structure and membrane affinity of new amphiphilic siderophores produced by Ochrobactrum sp. SP18. J. Biol. Inorg. Chem. **11:**633–641.
43. **Ito Y, Butler A.** 2005. Structure of synechobactins, new siderophores of the marine cyanobacterium Synechococcus sp. PCC 7002. Limnol. Oceanogr. **50:**1918–1923.
44. **Persmark M, Pittman P, Buyer JS, Schwyn B, Gill PR, Neilans JB.** 1993. Isolation and structure of rhizobactin 1021, a siderophore from the alfalfa symbiont Rhizobium meliloti 1021. J. Am. Chem. Soc. **115:**3950–3956.

45. **Ratledge C, Patel PV.** 1976. Isolation, properties and taxonomic relevance of lipid-soluble, iron-binding compounds (the nocobactins) from Nocardia. J. Gen. Microbiol. **93:**141–152.
46. **Stephan H, Freund S, Beck W, Jung G, Meyer JM, Winkelmann G.** 1993. Ornibactins—a new family of siderophores from Pseudomonas. Biometals **6:**93–100.
47. **Ratledge C.** 2004. Iron, mycobacteria and tuberculosis. Tuberculosis (Edinb.) **84:**110–130.
48. **Ihnat PM, Vennerstrom JL, Robinson DH.** 2000. Synthesis and solution properties of deferoxamine amides. J. Pharmacol. Sci. **89:**1525–1536.
49. **Barona-Gómez F, Lautru S, Francou FX, Leblond P, Pernodet JL, Challis GL.** 2006. Multiple biosynthetic and uptake systems mediate siderophore-dependent iron acquisition in Streptomyces coelicolor A3(2) and Streptomyces ambofaciens ATCC 23877. Microbiology **152:** 3355–3366.
50. **Barona-Gómez F, Wong U, Giannakopulos AE, Derrick PJ, Challis GL.** 2004. Identification of a cluster of genes that directs desferrioxamine biosynthesis in Streptomyces coelicolor M145. J. Am. Chem. Soc. **126:** 16282–16283.
51. **Smoot ME, Ono K, Ruscheinski J, Wang PL, Ideker T.** 2011. Cytoscape 2.8: new features for data integration and network visualization. Bioinformatics **27:**431–432.